Received: 2 July 2022 | Revised: 21 October 2022 | Accepted: 2 November 2022

DOI: 10.1111/mpp.13282

Molecular Plant Pathology WILEY

ORIGINAL ARTICLE

Turnip crinkle virus-encoded suppressor of RNA silencing interacts with *Arabidopsis* SGS3 to enhance virus infection

Linyu Liu[1,2] | Haiyan Wang[1] | Yan Fu[1] | Wen Tang[1] | Pingjuan Zhao[1] | Yanli Ren[2] | Zhixin Liu[1] | Kunxin Wu[1] | Xiuchun Zhang[1]

[1]Key Laboratory of Biology and Genetic Resources of Tropical Crops, Institute of Tropical Bioscience and Biotechnology, Chinese Academy of Tropical Agricultural Sciences & Key Laboratory for Biology and Genetic Resources of Tropical Crops of Hainan Province, Hainan Institute for Tropical Agriculture Resources, Haikou, China

[2]School of Biological and Geographical Sciences, Yili Normal University, Yili, China

Correspondence
Kunxin Wu and Xiuchun Zhang, Key Laboratory of Biology and Genetic Resources of Tropical Crops, Institute of Tropical Bioscience and Biotechnology, Chinese Academy of Tropical Agricultural Sciences & Key Laboratory for Biology and Genetic Resources of Tropical Crops of Hainan Province, Hainan Institute for Tropical Agriculture Resources, Haikou 571101, China.
Email: wukunxin@itbb.org.cn; zhangxiuchun@itbb.org.cn

Funding information
Central Public-interest Scientific Institution Basal Research Fund for Chinese Academy of Tropical Agricultural Sciences, Grant/Award Number: 19CXTD-33; Hainan basic and applied basic research program, Grant/Award Number: 321RC641 and 322MS124; National Natural Science Foundation of China, Grant/Award Number: 31570145 and 32070172

Abstract

Most plant viruses encode suppressors of RNA silencing (VSRs) to protect themselves from antiviral RNA silencing in host plants. The capsid protein (CP) of *Turnip crinkle virus* (TCV) is a well-characterized VSR, whereas SUPPRESSOR OF GENE SILENCING 3 (SGS3) is an important plant-encoded component of the RNA silencing pathways. Whether the VSR activity of TCV CP requires it to engage SGS3 in plant cells has yet to be investigated. Here, we report that TCV CP interacts with SGS3 of *Arabidopsis* in both yeast and plant cells. The interaction was identified with the yeast two-hybrid system, and corroborated with bimolecular fluorescence complementation and intracellular co-localization assays in *Nicotiana benthamiana* cells. While multiple partial TCV CP fragments could independently interact with SGS3, its hinge domain connecting the surface and protruding domains appears to be essential for this interaction. Conversely, SGS3 enlists its N-terminal domain and the XS rice gene X and SGS3 (XS) domain as the primary CP-interacting sites. Interestingly, SGS3 appears to stimulate TCV accumulation because viral RNA levels of a TCV mutant with low VSR activities decreased in the *sgs3* knockout mutants, but increased in the *SGS3*-overexpressing transgenic plants. Transgenic *Arabidopsis* plants overexpressing TCV CP exhibited developmental abnormalities that resembled *sgs3* knockout mutants and caused similar defects in the biogenesis of *trans*-acting small interfering RNAs. Our data suggest that TCV CP interacts with multiple RNA silencing pathway components that include SGS3, as well as previously reported DRB4 (dsRNA-binding protein 4) and AGO2 (ARGONAUTE protein 2), to achieve efficient suppression of RNA silencing-mediated antiviral defence.

KEYWORDS
antiviral RNA silencing, SUPPRESSOR OF GENE SILENCING3 (SGS3), tasi-RNA, turnip crinkle virus (TCV), viral suppressors of RNA silencing (VSR)

Linyu Liu and Haiyan Wang contributed equally.

1 | INTRODUCTION

RNA silencing or RNA interference (RNAi) refers to a number of mechanistically related pathways conserved in eukaryotic organisms ranging from fungi to humans (Jin et al., 2021). It is triggered by double-stranded RNA (dsRNA) or partially double-stranded hairpin RNA, digestion of which by a dsRNA-specific RNase (Dicer or DICER-LIKE [DCL] in plants) produces 21–24 nucleotide (nt) small interfering RNAs (siRNAs) or microRNAs (miRNAs) (Moissiard et al., 2007; Parent et al., 2015). In addition to DCLs, the early dsRNA-processing step frequently requires one member of the dsRNA-BINDING PROTEIN (DRB) family (Curtin et al., 2008; Hiraguri et al., 2005). siRNAs/miRNAs are then recruited into the RNA-induced silencing complex (RISC), directing ARGONAUTE (AGO) proteins in the complexes to cleave homologous RNAs (Huang et al., 2019; Jin et al., 2021). The amplification phase of RNA silencing requires RNA-dependent RNA polymerase 6 (RDR6) and SUPPRESSOR OF GENE SILENCING 3 (SGS3), which, in the form of SGS3/RDR6 bodies, coordinate the biogenesis of secondary siRNAs and endogenous *trans*-acting siRNA (tasiRNA) (Kumakura et al., 2009; Mourrain et al., 2000; Peragine et al., 2004; Yoshikawa et al., 2005, 2013). RNA silencing-mediated sequence-specific RNA degradation plays essential roles in combatting intracellular parasites, including viruses, and in endogenous biological processes such as plant development, maintenance of genome stability, and response to environmental stresses (Ding, 2010).

To counteract antiviral RNA silencing, most plant viruses have evolved one or more proteins, termed viral suppressors of RNA silencing (VSRs), to subdue RNA silencing at virtually all steps, such as viral RNA recognition, dicing, RISC formation, amplification, and RNA slicing (Chapman et al., 2004; Li & Wang, 2019; Yang & Li, 2018). Common strategies used by VSRs include siRNA sequestration and inactivation of AGO proteins through direct interaction or accelerated degradation. Various VSRs have also been found to target components of the amplification step of RNA silencing, including RDR6 and SGS3. For example, the P6 protein of rice yellow stunt virus (RYSV) binds to RDR6, interfering with the production of secondary siRNAs and systemic RNA silencing (Guo et al., 2013). Similarly, the V2 protein of tomato yellow leaf curl virus (TYLCV) and the p2 protein of rice stripe virus (RSV) were shown to interact with SGS3 (Du et al., 2011; Glick et al., 2008). The TGB1 protein of Plantago asiatica mosaic virus (PlAMV) was reported to co-aggregate with SGS3/RDR6 bodies (Okano et al., 2014), whereas the VPg protein of potyviruses and the nonstructural proteins (NSs) of *tomato zonate spot virus* (TZSV) were found to induce the degradation of SGS3 proteins, thereby blocking the amplification of the antiviral RNA silencing and attenuating plant antiviral immunity (Chen et al., 2022; Cheng & Wang, 2016; Rajamäki et al., 2014).

Turnip crinkle virus (TCV) is a member of the genus *Betacarmovirus*, family *Tombusviridae*. It is a small icosahedral virus with a single-stranded, positive-sense RNA genome that encodes five proteins. The 38 kDa capsid protein (CP), also known as P38, is needed for virus assembly and long-distance movement of the virus (Cao et al., 2010; Choi et al., 2004). TCV CP was previously found to overcome two separate defence barriers to facilitate TCV systemic movement in *Arabidopsis*, and also acts as a strong VSR in TCV-infected plants (Cao et al., 2010; Qu et al., 2003). It suppresses RNA silencing induced by both single- and double-stranded RNAs, preventing systemic silencing. In addition to suppressing DCL2 and DCL4 activities, TCV CP prevents RISC assembly through physical interactions with AGO1 (Azevedo et al., 2010). Furthermore, TCV CP was also reported to bind to dsRNA and siRNAs, thus preventing siRNAs from joining the RISC (Giner et al., 2010; Jin & Zhu, 2010). TCV CP was also found to prevent the processing of dsRNA produced by RDR6 (Iki et al., 2017). However, whether or not TCV CP targets the SGS3/RDR6 complex directly to further booster its VSR activity has not been investigated. In this report, we provide evidence showing that TCV CP physically interacts with SGS3 and the interaction plays a proviral role in TCV-infected plants.

2 | RESULTS

2.1 | TCV CP interacts with SGS3 at the sites of cytoplasmic bodies containing RDR6

Previous studies by others demonstrated that SGS3 interacts with RDR6 to form cytoplasmic SGS3/RDR6 bodies that are required for the amplification of RNA silencing and production of endogenous tasiRNAs (Kumakura et al., 2009; Mourrain et al., 2000; Peragine et al., 2004; Yoshikawa et al., 2005, 2013). We thus wondered whether TCV CP, a TCV-encoded VSR, interacted with SGS3 to boost TCV infection. We first used the yeast two-hybrid assay (Y2H) to test the potential interaction between the full-length TCV CP and SGS3 of *Arabidopsis*. As shown in Figure 1a, TCV CP and SGS3 readily interacted with each other in yeast cells, as indicated by robust yeast growth on quadruple dropout (QDO) medium when TCV CP and SGS3 were fused to the activation domain (AD) and DNA-binding domain (BD) vectors, respectively. CP and SGS3 did not exhibit any auto-activation or autobinding activity (Figure S1). The specific interaction between TCV CP and SGS3 was further corroborated by bimolecular fluorescence complementation (BiFC) assays. For this purpose *Arabidopsis* SGS3 was fused with an C-terminal green fluorescent protein (GFP) fragment at its own C-terminus, whereas TCV CP was fused with a N-terminal GFP fragment at its N-terminus, giving rise to SGS3-GC and GN-CP fusion proteins. SGS3-GC and GN-CP interacted with each other in *Nicotiana benthamiana* cells to form intracellular inclusions (Figure 1bI) that resembled the previously reported SGS3/RDR6 bodies (Figure S2I, serving as positive control), and also occurred at similar intracellular locations (Cheng & Wang, 2016; Kumakura et al., 2009), suggesting that TCV CP and SGS3 interacted with each other at or near SGS3/RDR6 bodies. Consistent with this, the distinct granule-like foci co-localized with RDR6-RFP, which served as a marker for SGS3/RDR6 bodies (Figure S3). No interaction was found between TCV CP and Mal co-expression (Figure S2II, serving as negative control; unless otherwise stated, these positive and negative control combinations would be included in all following BiFC experiments).

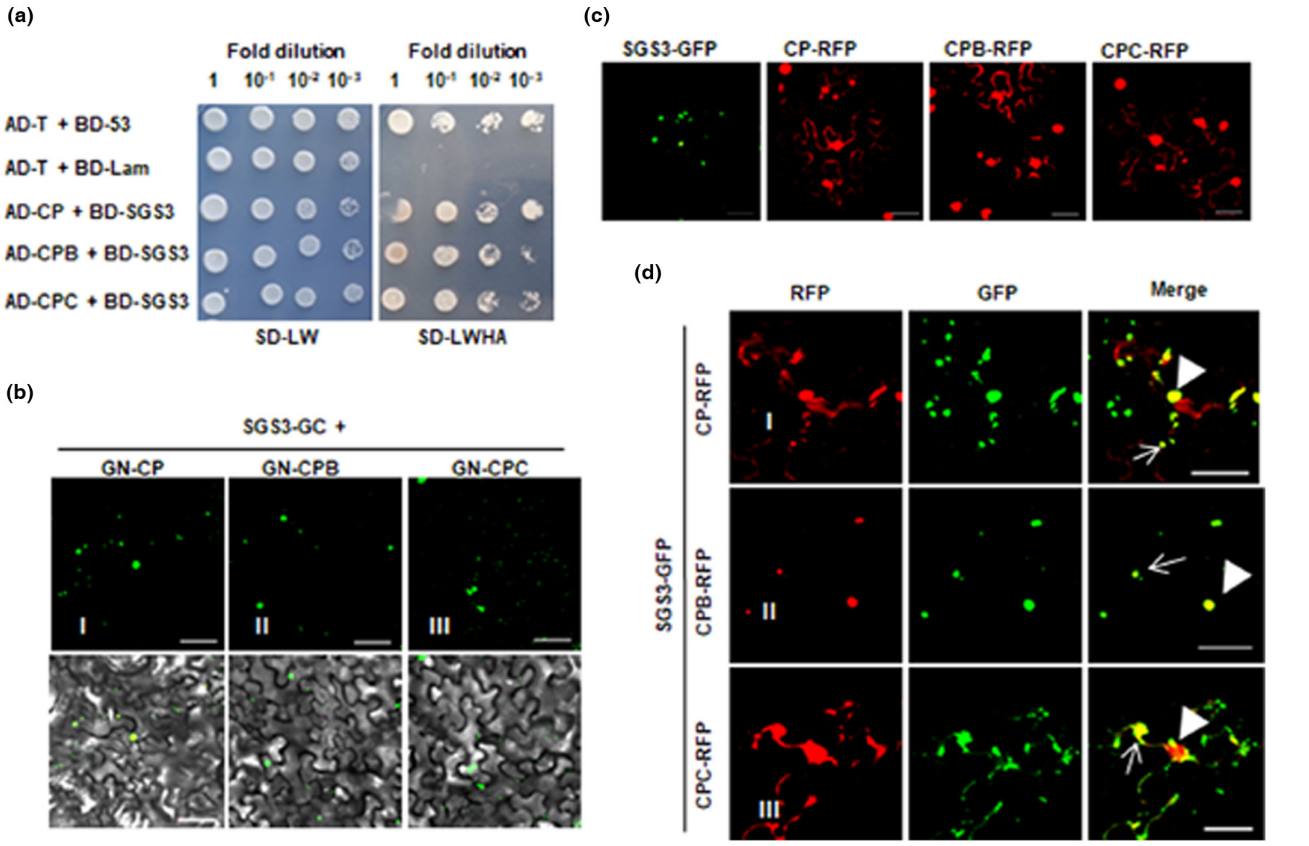

FIGURE 1 TCV capsid protein (CP) interacts with *Arabidopsis* SGS3. (a) Yeast two-hybrid assay for protein–protein interactions between TCV CP or its mutant CPB (R130T) or CPC (R137H) and SGS3 on selective media. The positive and negative controls are yeast co-transformants with pGAD-T plus pGBK-53 and pGAD-T plus pGBK-Lam, respectively. AD, GAL4 activation domain; BD, GAL4 DNA-binding domain; SD−LWHA, synthetic defined (SD) yeast minimal medium lacking Leu, Trp, His, and adenine hemisulphate. (b) Bimolecular fluorescence complementation assay for protein–protein interactions between TCV CP (i) or its mutant CPB (II) or CPC (III) and SGS3. TCV CP, CPB, and CPC were fused with the N-terminal, while SGS3 was fused with the C-terminal half of green fluorescent protein (GFP), designated as GN-CP, GN-CPB, GN-CPC, and SGS3-GC, respectively, and transiently expressed in *Nicotiana benthamiana* leaves. Fluorescence was monitored by confocal microscopy at 48 h postinoculation (hpi). Bar, 50 μm. (c) Subcellular localization of GFP fused with SGS3 (SGS3-GFP) or red fluorescent protein fused with CP (CP-RFP) or CPC (CPC-RFP). Bar, 50 μm. (d) Confocal micrographs of *N. benthamiana* co-expressing (CP-RFP) (I), CPB (CPB-RFP) (II) or CPC (CPC-RFP) (III) with SGS3-GFP at 48 h postinoculation. Bar, 50 μm. White arrowhead and white arrows indicate the nuclear and cytoplasmic interaction bodies, respectively

The CP–SGS3 interaction within the SGS3/RDR6 bodies of *N. benthamiana* epidermal cells was further corroborated with subcellular colocalization assays. As shown in Figure 1c, TCV CP with a C-terminal red fluorescent protein (RFP) fusion (CP-RFP) exhibited diffuse distribution, whereas SGS3 with a C-terminal GFP fusion (SGS3-GFP) showed discrete granule-like foci in the cytosol, as previous reported (Cheng & Wang, 2016). However, on co-expression in the same cells, CP-RFP coalesced into the cytoplasmic granules containing SGS3-GFP, as well as the cell nuclei (Figure 1dI), suggesting that the intracellular distribution of TCV CP was altered by its interaction with SGS3. Interestingly, this interaction also appeared to change the intracellular distribution of SGS3, as SGS3-GFP alone did not localize to cell nuclei.

To determine whether or not CP-SGS3 interaction was dependent on the VSR activity of TCV CP, we next tested TCV CP mutants with single amino acid substitutions (CPB and CPC, with mutations R130T and R137H, respectively) that diminished its VSR activities (Cao et al., 2010), for their potential interaction with SGS3. Y2H assays showed that both CPB and CPC still interacted with SGS3, and the interactions were as strong as the wild-type TCV CP based on the yeast growth (Figure 1a). The interactions between CPB/CPC and SGS3 were further corroborated with BiFC and subcellular co-localization assays (Figure 1b–d); therefore, both CPB and CPC mutations, although greatly weakening the VSR activity of TCV CP, did not abolish its interaction with SGS3.

2.2 | The five amino acid hinge connecting the surface and protruding domains of TCV CP is essential for SGS3 interaction

We next attempted to map the domains within TCV CP mediating the interaction with SGS3 using the Y2H assay. To this end, we tested four truncation mutants of TCV CP: RA (amino acids

1 to 82 consisting of the N-terminal RNA-binding [R] and arm [A] domains), RAS (amino acids 1–244 containing R, A, and surface [S] domains), RASH (amino acids 1–249 containing R, A, S, and hinge [H] domains), and SHP (amino acids 83–351 encompassing S, H and protruding [P] domains) (Cao et al., 2010) (Figure 2a). Y2H assays showed that both RASH and SHP mutants retained the ability to interact with SGS3 (Figure 2b). By contrast, the RA and RAS mutants were unable to interact with SGS3 (Figure 2b). Because the SGS3-interacting RASH fragment differed from the noninteracting RAS fragment by only the five amino acid H domain, these results mapped the SGS3-interacting domain in TCV CP to the five amino acid H domain. These results were corroborated with the BIFC assay (Figure 2cI,II). Unexpectedly, RAS and RA reconstituted the GFP signal when co-expressed with SGS3 in the BiFC assay (Figure 2cIII,IV) while all the truncated versions of CP did not reconstitute the GFP signal when co-expressed with Mal, which serves as a negative control (Figure S2II–VI), suggesting that RA and RAS mutants might interact with SGS3 but the intensity of interaction was not strong enough for yeast growth. Together these data identified a five amino acid region within TCV CP as the main determinant for interacting with SGS3.

2.3 | The NTD and XS domains of SGS3 mediate its interaction with TCV CP

We next attempted to map the TCV CP-interacting domain(s) in SGS3. Based on its predicted domain structure, we generated four SGS3 deletion mutants, each containing one of the four predicted domains: the N-terminal domain (SGS3-NTD, amino acids 1–200), the zinc finger domain (SGS3-ZF, amino acids 201–289), the rice gene X and SGS3 domain (SGS3-XS, amino acids 290–411), and the

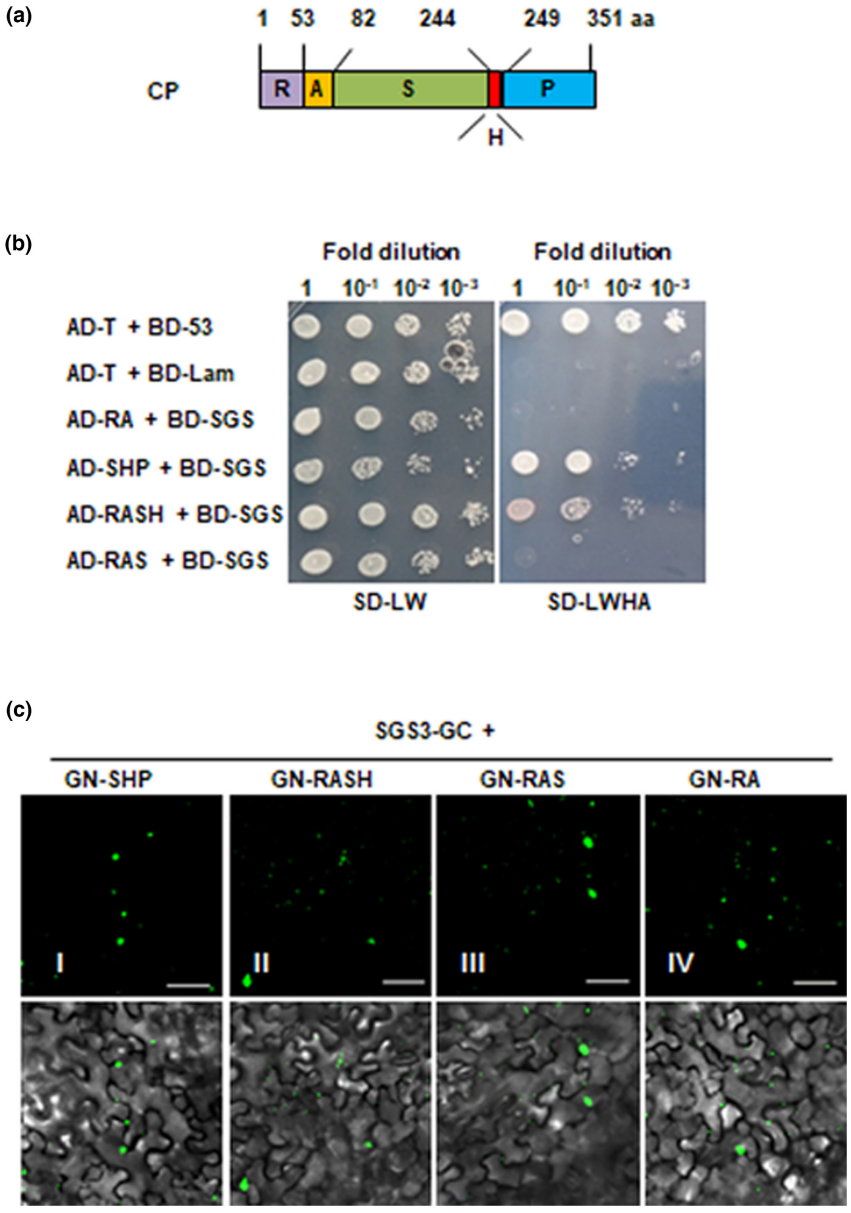

FIGURE 2 Mapping of the interaction domains in the TCV capsid protein (CP) and SGS3. (a) Schematic representation of full-length CP, with the sizes and relative positions of the five structural domains shown. The numbers at the top are the positions of the first amino acids of the respective domains and the last amino acid of the whole CP. R, RNA-binding domain; a, arm; S, surface domain; H, hinge; P, protruding domain. (b) Yeast two-hybrid assay for protein–protein interactions of BD-SGS3 with AD-RA, AD-SHP, AD-RASH, or AD-RAS on selective media. The positive and negative controls are the yeast co-transformants with pGAD-T plus pGBK-53 and pGAD-T plus pGBK-Lam, respectively. AD, GAL4 activation domain; BD, GAL4 DNA-binding domain; SD−LWHA, synthetic defined (SD) yeast minimal medium lacking Leu, Trp, His, and adenine hemisulphate in yeast cells. (c) The interaction between truncated CPs and SGS3 was confirmed by bimolecular fluorescence complementation assays. Truncated CPs including SHP, RASH, RAS, and RA were fused with the N-terminal, while SGS3 was fused with the C-terminal half of green fluorescent protein (GFP), designated as GN-SHP, GN-RASH, GN-RAS, GN-RA, and SGS3-GC, respectively, and transiently expressed in *Nicotiana benthamiana* leaves. Bars, 50 μm

C-terminal coiled-coil (CC) domain (SGS3-CC, amino acids 412–625) (Cheng & Wang, 2016) (Figure 3a). When the GFP-tagged forms of these mutants were expressed in *N. benthamiana* leaves alone via agroinfiltration, the green fluorescence was diffused in the cytoplasm and nuclei of the treated cells (Figure 3b), differing from the full-length SGS3-GFP, which were exclusively found in the cytoplasmic granules (Figure 1c). These results suggest that more than one of the four SGS3 domains are needed for it to form cytoplasmic granules.

We next used the Y2H assay to reveal that all four SGS3 domains could interact with TCV CP. SGS3-NTD or SGS3-XS interacted with TCV CP much more strongly than SGS3-ZF or SGS3-CC, as indicated by more rapid yeast growth (Figure 3c). Consistent with these results, SGS3-NTD, SGS3-XS, SGS3-ZF, and SGS3-CC reconstituted the GFP signal when co-expressed with TCV CP in the BiFC assay (Figure 3d). The results indicate the presence of multiple TCV CP-interacting sites on SGS3, with the NTD and XS domains as the main determinants.

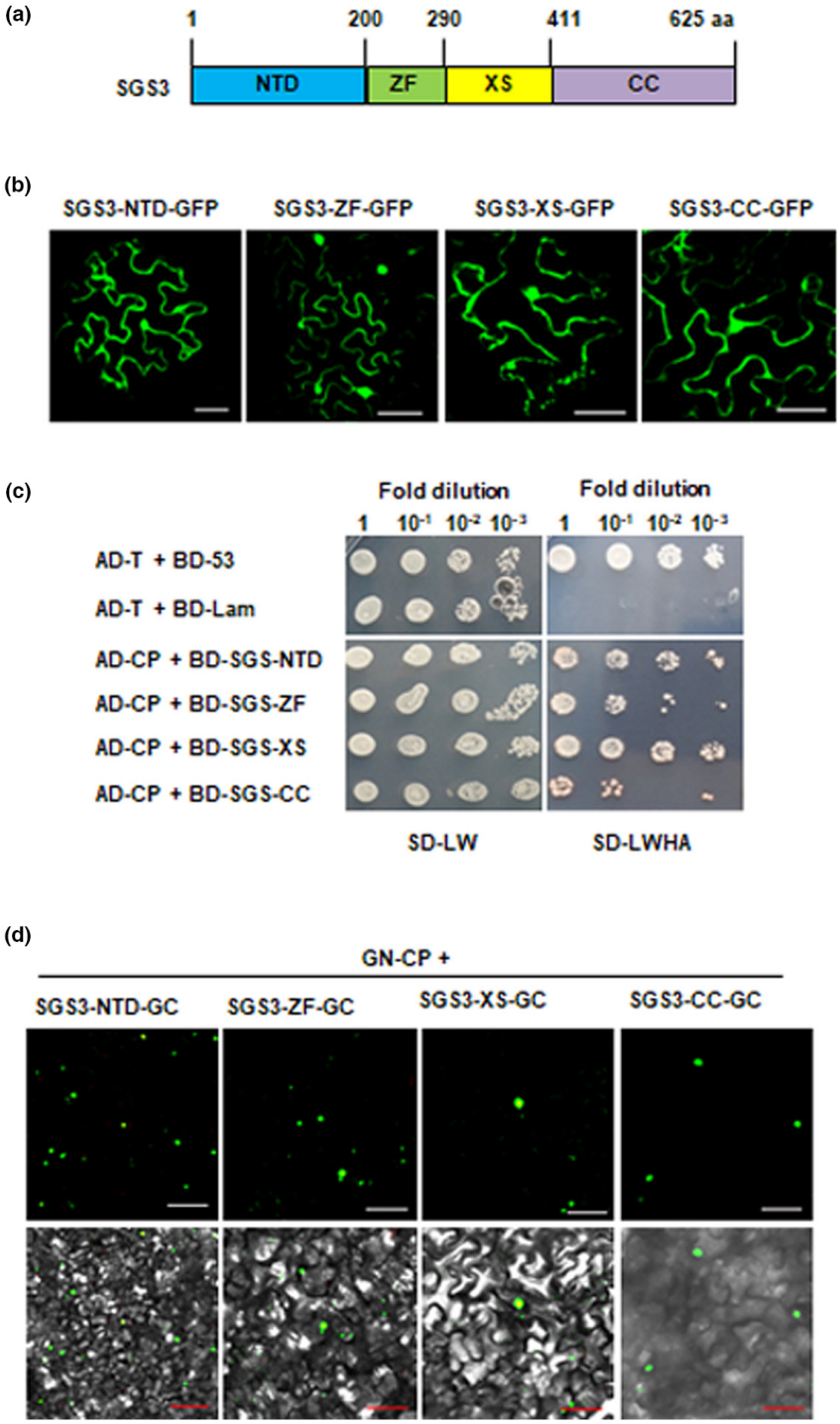

FIGURE 3 Mapping of the interaction domains in SGS3. (a) Schematic representations of SGS3. NTD, SGS3 N-terminal domain; ZF, putative SGS3 zinc finger domain; the rice gene X and SGS3 domain (SGS3-XS) domain; CC, SGS3 coiled-coil domain. The numbers represent amino acid positions of domain boundaries. (b) Subcellular localization of mCherry fused with TCV capsid protein (CP-RFP) or green fluorescent protein (GFP) fused with their truncated SGS3 domains in *Nicotiana benthamiana* as indicated. Bar, 50 μm. (c) Yeast two-hybrid assay for protein–protein interactions of AD-CP with BD-SGS-NTD, BD-SGS-ZF, BD-SGS-XS, or BD-SGS-CC on selective media. The positive and negative controls are the yeast co-transformants with pGAD-T plus pGBK-53 and pGAD-T plus pGBK-Lam, respectively. AD, GAL4 activation domain; BD, GAL4 DNA-binding domain; SD−LWHA, synthetic defined (SD) yeast minimal medium lacking Leu, Trp, His, and adenine hemisulphate In yeast cells. (d) The interaction between CP and each of the four truncated SGS3 domains was confirmed by bimolecular fluorescence complementation assay. TCV CP was fused with the N-terminal, while the truncated SGS3 domains were fused with the C-terminal half of GFP, designated as GN-CP SGS-NTD-GC, SGS-ZF-GC, SGS-XS-GC, and SGS-CC-GC, respectively, and transiently expressed in *N. benthamiana* leaves. Bars, 50 μm

2.4 | TCV CP does not disrupt the interaction between SGS3 and RDR6

Previous studies by others established that SGS3 and RDR6 interact with each other to form small cytoplasmic bodies designated as SGS3/RDR6 bodies or siRNA bodies (Kumakura et al., 2009). To assess the biological relevance of the interactions between TCV CP and SGS3, we next investigated whether TCV CP negatively regulates the assembly of the SGS3/RDR6 bodies. To this end, GN-RDR6 and GC-SGS3 were co-infiltrated with an empty vector, TCV CP, or TCV CPC into *N. benthamiana* leaves. As shown in Figure 4a, the GFP signal could be reconstituted in cells co-infiltrated with the empty vector, but also with TCV CP and TCV CPC, suggesting that TCV CP and TCV CPC did not disrupt the assembly of SGS3/RDR6 bodies. The subcellular colocalization of SGS3 and RDR6 was also verified by transiently co-expressing SGS3-GFP and RDR6-RFP in the presence of an empty vector, TCV CP, or TCV CPC. As shown in Figure 4b, SGS3 and RDR6 colocalization was observed in both cases, confirming that TCV CP and TCV CPC could not disrupt the assembly of SGS3/RDR6 bodies.

2.5 | SGS3 enhances TCV RNA accumulation

To assess the biological relevance of CP-SGS3 interaction, we infected two SGS3 knockout *Arabidopsis* lines, *sgs3-12* and *sgs3-14*, with in vitro transcribed infectious RNA of CPB. Surprisingly, the CPB RNA levels decreased in inoculated leaves (ILs) of both *sgs3-12* and *sgs3-14* mutants (Figure 5a, lanes 7,8, and 1, TRNA blot). The reduction of CPB RNA levels was discernable when the inoculated plants were kept at 26°C (Figure 5a left panel) and was even more pronounced at 18°C (Figure 5a right panel). Therefore, abolishing

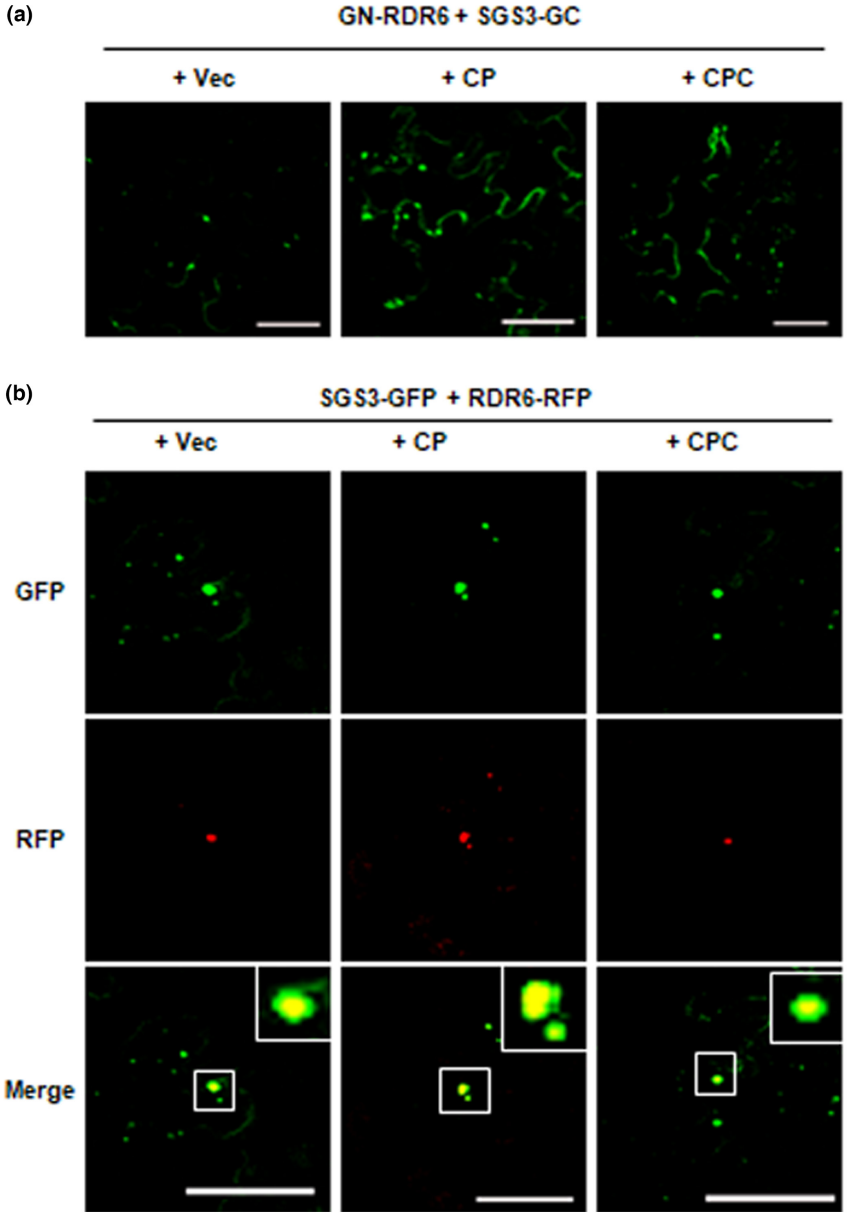

FIGURE 4 TCV capsid protein (CP) could not disrupt the interaction between SGS3 and RDR6. (a) Bimolecular fluorescence complementation (BiFC) assays for GN-RDR6 and GC-SGS3 interaction in the presence of an empty vector (+Vec), CP (+CP), or CPC (+CPC). (b) Colocalization of SGS3-GFP and RDR6-RFP in the presence of an empty vector (+Vec), CP (+CP), or CPC (+CPC). BiFC and colocalization assays were carried out in wild-type *Nicotiana benthamiana* leaf cells. Confocal microscopy was carried out at 32 h postinoculation. Insets show the co-localization of SGS3-GFP and RDR6-RFP. GFP, green fluorescent protein; RFP, red fluorescent protein. Bars, 50 μm

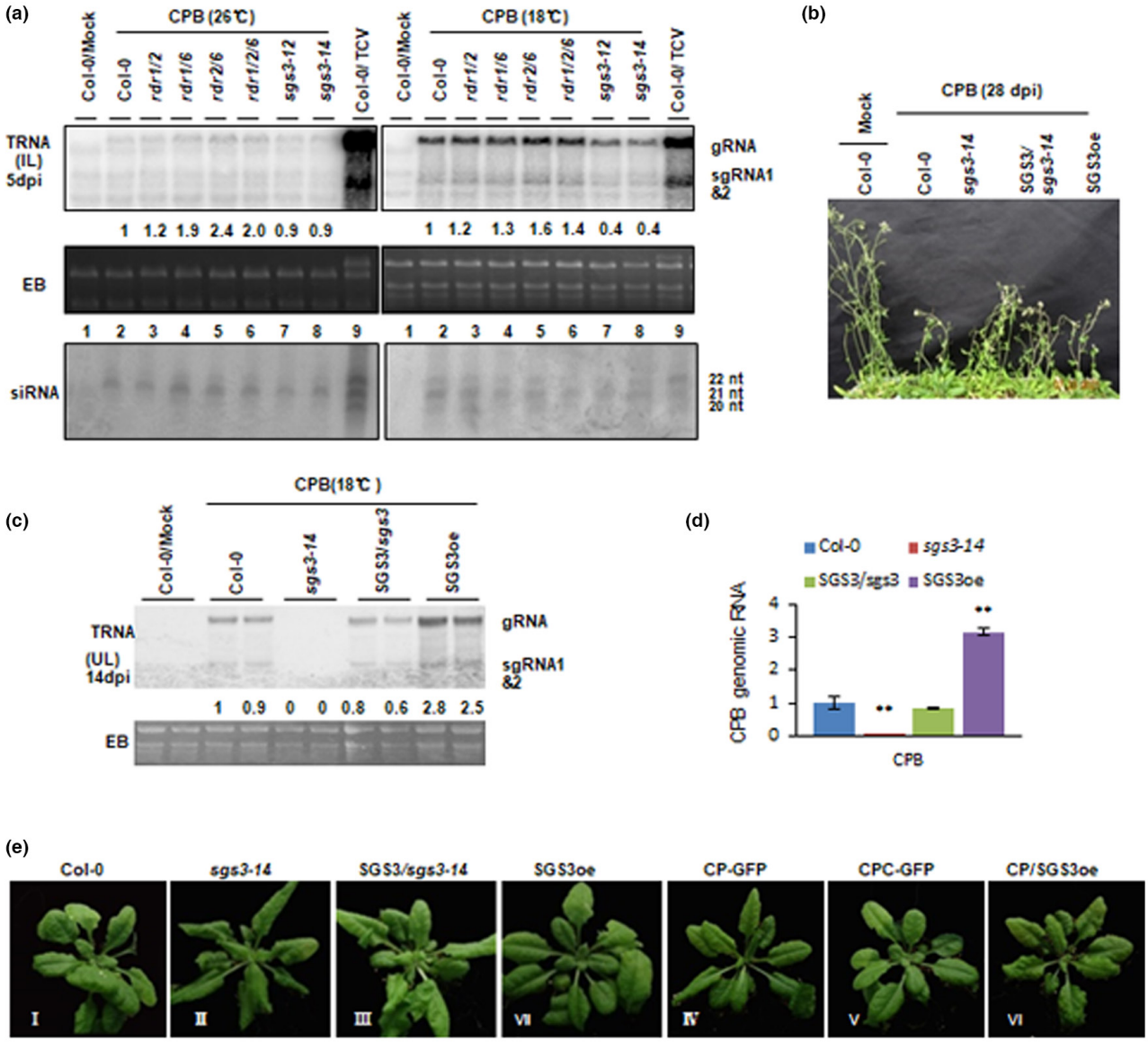

FIGURE 5 TCV accumulation is positively correlated with *sgs3* mRNA levels in *Arabidopsis* plants, while RDR6 is required for efficient antiviral RNA silencing. (a) Detection of CPB gRNA, sgRNAs, and vsRNAs by northern blot hybridizations in inoculated leaves (IL) from Col-0, *rdr1/2*, *rdr1/6*, *rdr2/6*, *rdr1/2/6*, *sgs3-12*, and *sgs3-14* plants, which were kept at 26 and 18°C as indicated. The probe was a mix of five [^{32}P]-labelled oligonucleotides complementary to TCV genomic RNA (gRNA). EB, ethidium bromide-stained northern gel; sgRNA, subgenomic RNA. See Qu et al. (2008) for a detailed procedure. (b) Phenotype of CPB-infected *Arabidopsis* plants as indicated. Col-0, *sgs3-14* mutant, SGS3-overexpressing transgenic *Arabidopsis* plant in Col-0 background (SGS3oe), and SGS3 restored transgenic *Arabidopsis* plant in *sgs3-14* mutant background (SGS3/sgs3) plants. Images were obtained at 28 days postinoculation. (c) Northern blot hybridization of the total RNAs extracted from the upper uninoculated leaves (ULs) of CPB-infected *Arabidopsis* Col-0, *sgs3-14* mutant, SGS3 restored transgenic plant (SGS3/*sgs3-14*), and SGS3-overexpressing transgenic plant (SGS3oe) plants. Each RNA sample was extracted from six ULs pooled from six plants. To eliminate variabilities, we analysed two different RNA samples per treatment. The probe was digoxygenin (DIG)-labelled DNA, which is a 667-nucleotide fragment of TCV. EB, ethidium bromide-stained northern gel; sgRNA, subgenomic RNA. See Wu et al. (2021) for a detailed procedure. (d) Droplet digital PCR (ddPCR) analysis of viral RNA accumulation in the ULs of CPB-infected *Arabidopsis* Col-0, *sgs3-14* mutant, SGS3 restored transgenic plant (SGS3/sgs3), SGS3-overexpressing transgenic plant (SGS3oe) plants. Each RNA sample was extracted from six ULs pooled from six plants. Expression is normalized against the *AtActin1* gene, which was used as an internal control. All values are expressed as means ± *SD* from three independent biological replicates, and asterisks denote significant differences from the control group (*$p < 0.05$, **$p < 0.01$). (e) Phenotypes of Col-0, *sgs3-14* mutant, SGS3 restored transgenic *Arabidopsis* plants (SGS3/sgs3), SGS3-overexpressing (SGS3oe) transgenic *Arabidopsis*, plants transformed with 35S:CP-GFP (CP-GFP) or 35S:CPC-GFP (CPC-GFP), and F_2 generation heterozygous plants obtained by crossing homozygous CP-GFP plants with SGS3oe plants (CP/SGS3oe)

SGS3 functionality counterintuitively enhanced the plant resistance to CPB infection.

To further assess how CPB RNA levels were regulated by SGS3, we generated transgenic plants that overexpress a FLAG-tagged SGS3 (FLAG-SGS3) in both Col-0 (wild type) and *sgs3-14* backgrounds. The resulting transgenic plants were designated as SGS3oe and SGS3oe/*sgs3*, respectively. The expression of SGS3-FLAG in transgenic plants was confirmed by western blot analysis (Figure S4a). Consistent with previous reports (Cheng & Wang, 2016), SGS3 overexpression did not affect normal plant development under our growth conditions (Figure 5e). Furthermore, SGS3oe/*sgs3* plants partially corrected the abnormal phenotype of *sgs3-14* mutant (Figure 5e).

Four-week-old seedlings of the homozygous SGS3oe and SGS3oe/*sgs3* along with *sgs3-14* and Col-0 plants were mechanically inoculated with in vitro transcribed infectious RNA of CPB. The inoculated plants were kept at 18°C. Col-0, *sgs3-14*, SGS3oe/*sgs3*, and SGS3oe plants developed typical TCV symptoms such as substantially reduced stature, while *sgs3-14* plants showed the mildest symptoms as indicated by the highest growth among all infected plants at 28 days postinoculation (dpi) (Figure 5b). Northern blot hybridizations showed that the CPB RNAs accumulated to lower levels in *sgs3-14* plants than in their wild-type counterparts (Figure 5c). Importantly the reduction of CPB RNA levels caused by the *sgs3* knockout mutation was reversed in transgenic SGS3oe/*sgs3* plants. Even more strikingly, CPB RNA levels were elevated in the transgenic plants overexpressing SGS3 (SGS3oe). The CPB RNA levels in these plants were further quantified with droplet digital PCR (ddPCR), and the results (Figure 5d) were consistent with those of northern blot hybridization (Figure 5c). Collectively, the results suggest that SGS3 plays a negative regulatory role in antiviral silencing targeting CPB.

The profile of CPB-specific siRNAs was generally consistent with previous reports (Qu et al., 2008; Zhang et al., 2012). Their size was predominantly 21 nt (Figure 5a, siRNA blot). The relative concentration of siRNAs in these plants was roughly proportional to that of viral RNA, therefore wild-type plants infected with TCV contained the highest siRNA (Figure 5a, lane 9), plants with *rdr6* mutation infected with CPB contained less siRNA (Figure 5a, lanes 4–6), while *sgs3-12* and *sgs3-14* mutant infected plants contained the least (Figure 5a, lanes 7 and 8). Hence, in the mutants tested, the siRNA levels indicate the ongoing siRNA production from viral RNAs rather than the difference that resulted in siRNA amplification.

2.6 | TCV infection up-regulates the expression of *SGS3*, *DCL4*, and *RDR6*, but also the target genes of endogenous tasiRNAs

In addition to participating in antiviral defence, SGS3, RDR6, and DCL4 are needed for the biogenesis of tasiRNAs (Mourrain et al., 2000; Peragine et al., 2004; Yoshikawa et al., 2005). We hence examined whether TCV infection perturbed the expression of *DCL4*, *SGS3*, and *RDR6*, three proteins essential for tasiRNA biogenesis, as well as several genes known to be targets of tasiRNAs, including the *HEAT-INDUCED TAS1 TARGET 2* (*HTT2*, At5g18040), *AUXIN RESPONSE TRANSCRIPTION FACTOR* 3 (*ARF3*), and *ARF4* (Peragine et al., 2004). To eliminate the effect of functional redundancy of DCL2, we infected *dcl2 drb4* double knockout mutant plants with in vitro transcribed infectious RNA of TCV mutant CPB1B, which could induce PDS silencing, causing easily visible photobleaching in systemically infected *Arabidopsis* leaves (Wu et al., 2021), and the inoculated plants were kept at 18°C. ULs were collected from the plants at 14 dpi and subjected to RNA extraction and reverse transcription-quantitative PCR (RT-qPCR) using gene-specific primers (Table S5). CPB1B infection in the samples was verified by the visible photobleaching in the upper uninoculated leaves (ULs) (Figure S5a) and semiquantitative RT-PCR (Figure S5b).

The results of RT-qPCR analysis showed that the expressions of *DCL4*, *SGS3*, and *RDR6* mRNA were up-regulated in CPB1B-infected leaves, implying that these genes might be involved in anti-TCV defence (Figure 6a). However, despite the elevated levels of these genes, their functionality in the tasiRNA biogenesis pathway was apparently disrupted by TCV infection. This is because the mRNA levels of three genes targeted by tasiRNAs, *HTT2*, *ARF3* and *ARF4*, were also up-regulated, suggesting that the corresponding tasiRNAs were prevented from engaging their target mRNAs in the presence of TCV infection (Okano et al., 2014) (Figure 6b).

2.7 | Transgenic expression of TCV CP elevates the expression of *DCL4*, *SGS3*, *RDR6*, and targets of tasiRNAs

To further determine how TCV infection up-regulates the expression of the tasiRNA pathway genes, we generated transgenic *Arabidopsis* plants that express GFP-tagged TCV CP or CPC CP, which were confirmed by confocal microscopy (Figure S4c), designated as CP-GFP or CPC-GFP, respectively. The CP-GFP plants (Figure 5eIV) exhibited obvious developmental defects in leaves, displaying downward-curled leaf margins similar to the *sgs3-14* mutant (Figure 5eII). By contrast, CPC-GFP-expressing plants had no discernible abnormality (Figure 5eV), indicating a correlation between the phenotype and the VSR activity of the TCV CP protein.

We next wondered whether the abnormal phenotype of CP-GFP transgenic plants could be antagonized by overexpressing SGS3. We hence generated CP/SGS3oe plants that overexpressed both SGS3 and CP by crossing CP-GFP transgenic plants with SGS3oe plants. The F_2 CP/SGS3oe plants with both transgenes were confirmed by genotyping (Figure S4b). As shown in Figure 5eVI, this indeed partially remedied the abnormal phenotype induced by CP-GFP expression, indicating that SGS3 overexpression could antagonize TCV CP to restore tasiRNA functionality in these plants.

Considering that the downward curling of leaf margins is a characteristic phenotype of tasiRNA-deficient mutants such as *sgs3*, *dcl4*, *ago7*, and *rdr6* (Peragine et al., 2004), TCV CP may disrupt a certain step in the tasiRNA pathway. To test whether the expression of TCV CP could suppress the function of SGS3 in tasiRNA biogenesis, we next

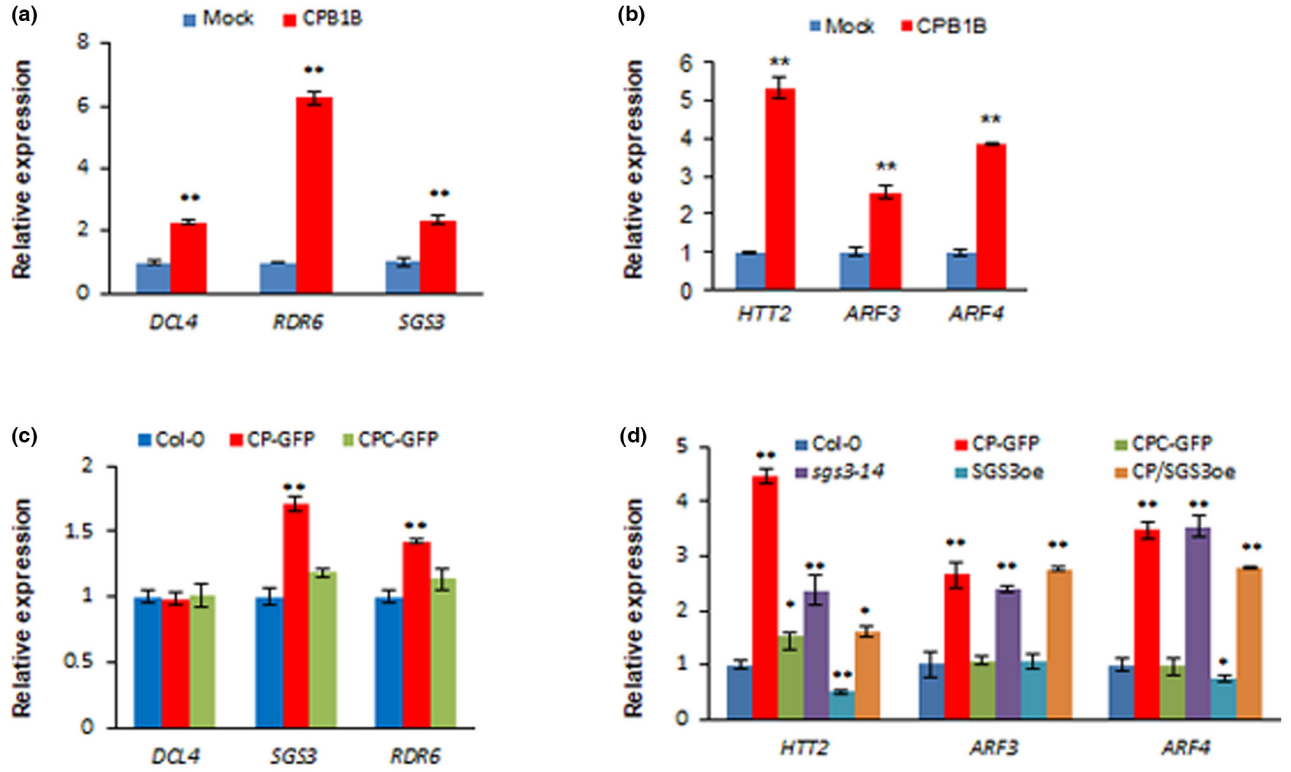

FIGURE 6 TCV infection and overexpressing capsid protein (CP) up-regulate the expression of *DCL4*, *SGS3*, *RDR6*, and the conserved primary transcripts of tasiRNA targets. (a, b) Reverse transcription-quantitative PCR (RT-qPCR) analysis of *DCL4*, *SGS3*, and *RDR6* expression levels (a), and *HTT2*, *ARF4*, and *ARF4* expression levels, which are conserved primary transcripts of tasiRNA targets (b) in *dcl2 drb4* double mutant newly emerged leaves of mock- or CPB1B-infected plants at 14 days postinoculation. Expression is normalized against the *AtActin*1 gene, which was used as an internal control. All values are expressed as means ± *SD* from three independent biological replicates, and asterisks denote significant difference from the control group (*$p < 0.05$, **$p < 0.01$). (c) RT-qPCR analysis of *DCL4*, *SGS3*, and *RDR6* expression levels in the Col-0, transgenic *Arabidopsis* plants transformed with 35S:CP-GFP (CP-GFP) or 35S:CPC-GFP (CPC-GFP). (d) RT-qPCR analysis of *HTT2*, *ARF4*, and *ARF4* expression levels, which are conserved primary transcripts of tasiRNA targets in Col-0, transgenic *Arabidopsis* plants transformed with 35S:CP-GFP (CP-GFP) or 35S:CPC-GFP (CPC-GFP), *sgs3-14* mutant, SGS3-overexpressing transgenic *Arabidopsis* plants (SGS3oe), and F_2 generation heterozygous plants obtained by crossing homozygous CP-GFP plants with SGS3oe plants (CP/SGS3oe)

investigated the effect of CP-GFP and CPC-GFP expression on the mRNA levels of *DCL4*, *SGS3*, *RDR6*, *HTT2*, *ARF3*, and *ARF4*. RT-qPCR results showed that CP-GFP expression substantially up-regulated the expression of *SGS3* and *RDR6*, but had no effect on that of *DCL4*. BY contrast, CPC-GFP overexpression had no effect on *DCL4*, *SGS3*, and *RDR6* mRNA levels (Figure 6c). Similarly, the *HTT2*, *ARF3*, and *ARF4* mRNA levels were dramatically elevated by CP-GFP transgenic expression. The extent of elevation was comparable to that of *sgs3-14* mutants. Notably, the CP-GFP-induced up-regulation of tasiRNA target genes was abolished by SGS3 overexpression (Figure 6d), strongly suggesting that TCV CP perturbs the tasiRNA pathway by targeting SGS3. Interestingly, CPC-GFP expression of TCV CPC only affected the expression of *HHT2*. In summary, TCV CP interfered with the endogenous tasiRNA biogenesis pathway by targeting SGS3.

3 | DISCUSSION

The SGS3/RDR6 complex has been found to play critical roles in antiviral RNA silencing by amplifying viral siRNAs (Dalmay et al., 2000; Kumakura et al., 2009; Mourrain et al., 2000; Muangsan et al., 2004; Peragine et al., 2004). This amplification step uses the viral RNAs already cleaved by primary RISCs as the templates to synthesize dsRNA, from which more siRNAs are produced through DCL4-mediated dicing. However, antiviral defence is not the only role for the SGS3/RDR6 complex. Previous studies by others demonstrated that SGS3/RDR6 complexes are also needed for the biogenesis of tasiRNAs, a class of endogenous secondary siRNAs that regulate plant development and responses to abiotic stresses (Peragine et al., 2004; Yoshikawa et al., 2005). It was further suggested that SGS3 plays the role of guiding RDR6 to a special class of endogenous RNA templates and to synthesize dsRNAs using this class of templates exclusively (Yoshikawa et al., 2021). Specifically, this class of endogenous RNAs must have undergone RISC cleavage mediated by a subclass of miRNAs that are 22 nt in size, therefore SGS3 not only assists RDR6 in dsRNA synthesis, but also ensures such dsRNA synthesis does not occur indiscriminately on other cellular RNAs not destined for degradation (Yoshikawa et al., 2021).

SGS3/RDR6-mediated amplification of viral siRNAs has been shown to play important antiviral roles in the infections of several

viruses, including TZSV (Chen et al., 2022), turnip mosaic virus (Cheng & Wang, 2016), TYLCV (Glick et al., 2008; Li et al., 2017), rice stripe mosaic virus (Zhang et al., 2020), cucumber mosaic virus (Wang et al., 2011), PlAMV (Okano et al., 2014), sweet potato chlorotic stunt virus (Weinheimer et al., 2016), and RSV (Du et al., 2011). Whether it also exerts a meaningful role in defence against TCV has not been carefully studied. TCV is unique in that it encodes an extremely strong VSR that almost completely shuts down the primary RNA silencing pathway (Qu et al., 2003). Indeed, we showed earlier that infection by wild-type TCV encoding the full strength VSR (CP) in wild-type Col-0, *dcl4*, *dcl2*, *dcl2*, and *dcl4* plants caused similar symptoms and similar levels of viral RNA (Cao et al., 2010; Qu et al., 2008; Zhang et al., 2012). Consistently, we showed that infection by wild-type TCV encoding the full-strength VSR (CP) in wild-type Col-0, *rdr1/2*, *rdr1/6*, *rdr2/6*, *rdr1/2/6*, *sgs3-12*, and *sgs3-14* plants caused similar symptoms and similar levels of viral RNA (Figure S6). As a result, anti-TCV roles of DCL4, DCL2, DRB4, AGO1, and AGO2 could only be revealed with TCV mutants that encode a drastically weakened VSR, such as CPB and CPC (Qu et al., 2008; Zhang et al., 2012).

In the current study, we identified a highly specific interaction between the TCV-encoded VSR (CP) and *Arabidopsis* SGS3 (Figure 1), and mapped the critical interacting domain in CP to a five amino acid region (Figure 2). We also used BiFC and colocalization assay to demonstrate that the intracellular sites of CP-SGS3 interaction colocalized with the SGS3-RDR6 complexes (Figures 3b and S3) and did not disrupt the SGS3-RDR6 interaction (Figure 4a,b). Surprisingly, while *rdr6* knockout mutant plants accumulated slightly more viral RNAs of CPB (Figure 5a), suggesting a relatively modest, but positive, antiviral role for RDR6, the *sgs3* knockout mutant plants actually accumulated measurably less CPB viral RNAs (Figure 5a,c,d), revealing a novel negative-regulating role of SGS3 in antiviral defence. Consistent with this observation, transgenic *Arabidopsis* plants overexpressing *SGS3* accumulated more CPB viral RNAs.

How do we explain this seemingly counterintuitive finding? We hypothesize that absence of SGS3 in *sgs3* mutants releases RDR6 from the template specificity conferred through SGS3, allowing RDR6 to engage other aberrant viral RNAs for dsRNA synthesis, leading to the production of more viral siRNAs, hence more robust degradation of viral RNAs. Conversely, SGS3 overexpression exerts stricter constraints on the kind of aberrant viral RNAs that can be used by RDR6 for dsRNA synthesis, thus lessening the activity of secondary RNA silencing against viral RNAs. This hypothesis will be tested in-depth in our future studies.

4 | EXPERIMENTAL PROCEDURES

4.1 | Plant materials and TCV variants

All *Arabidopsis thaliana* and *N. benthamiana* plants were grown in pots in a growth chamber at 23°C with 14 h of daylight and 60% humidity. The *dcl2 drb4*, *rdr1/2*, *rdr1/6*, *rdr2/6*, *rdr1/2/6*, *sgs3-12*, and *sgs3-14* mutants were provided by Feng Qu at Ohio State University. Homozygous mutation lines were screened by using the primers listed in Table S4. The *Arabidopsis* plants were inoculated with in vitro transcribed viral RNA at the age of 3–4 weeks. After inoculation, the infected plants were moved into a versatile environmental test chamber (SANYO) set at 18 or 26°C under a 16-h/8-h photoperiod with 60% humidity and light intensity of 160–190 $\mu mol\, m^{-2}\, s^{-1}$. *Arabidopsis* (ecotype Col-0 or *sgs3-14* mutant) plants were transformed via the floral-dip method. Transformants were screened by Murashige and Skoog (MS) medium supplied with 20 μg/ml hygromycin B, and then further confirmed by PCR.

The infectious clones CPB and CPC contain a single amino acid change at amino acid residues 130 (R130T) and 137 (R137H) of TCV CP, respectively, which was constructed in Dr Qu's laboratory at Ohio State University as previously described (Cao et al., 2010). The infectious clone CPB1B is a CPB-derived construct harbouring a 46-nt phytoene desaturase (*PDS*) fragment in the antisense orientation (Wu et al., 2021).

4.2 | Plasmid construction

For Y2H assay, the full-length coding sequences of *Arabidopsis RDR6* (AT3G49500) and *SGS3* (At5g23570) were obtained by RT-PCR using the primers designed based on the published sequence (Table S1). The amplified fragments were cloned into the vector pMD18T and confirmed by DNA sequencing, and then were subcloned in-frame with the GAL4 DNA BD in the vector pGBKT7. The deletion mutants of AtSGS3 (SGS3-NTD [amino acids 1–200], SGS3-ZF [amino acids 201–289], SGS3-XS [amino acids 290–411], and SGS3-CC [amino acids 412–625]) were amplified from the full-length SGS3 with appropriate nucleotide primers (Table S1) and were cloned in the vector pGBKT7. The full-length coding sequences of TCV CP and its truncated mutants CPRA, CPRAS, CPRASH, and CPSHP, which contain the N-terminal domain RA (amino acids 1–82), RAS (amino acids 1–244), RASH (amino acids 1–249), and C-terminal domain SHP (amino acids 83–351) were amplified from the pTCV (previously T1d1) construct with appropriate nucleotide primers (Table S1). The amplification products were cloned in-frame with the GAL4 DNA AD in the vector pGADT7. All the constructed plasmids were confirmed by DNA sequencing.

For BiFC experiments, pGN1 and p2GC were used to accommodate the cDNAs of various viral and plant proteins. pGN1 was modified from pG1300 (Ruan et al., 2017) by replacing the synthetic GFP fragment with N-terminal 159 amino acid residues of GFP and a haemagglutinin (HA) epitope tag (denoted as 1), which was amplified from pG1300 with primers GN1-F and GN1-R (Table S2). p2GC was constructed by replacing the GFP of pG1300 with a synthetic fragment, designated as GC-FLAG, which included C-terminal 81 amino acid residues of GFP and a FLAG epitope tag (denoted as 2) (Table S2). The HA and FLAG epitope tags were sandwiched by the partial fragment of GFP and the cDNAs to be examined, therefore the cDNAs to be examined

were always fused with an N-terminal GFP fragment at its own N-terminus in pGN1, while fusing with a C-terminal GFP fragment at its own C-terminus in p2GC. The full-length coding sequences of *Arabidopsis* Mal (AT3G47520.1) were obtained by RT-PCR using the primers designed based on the published sequence (Table S3). The amplified fragments were cloned into the vector pMD18T and confirmed by DNA sequencing, and then were subcloned in-frame with the binary vectors pGN1 or p2GC. The full-length *SGS3*, *RDR6*, *CP*, and truncated fragments were amplified from the yeast AD or BD constructs mentioned above with appropriate nucleotide primers (Table S3).

To determine the subcellular localization of various viral and plant proteins, we used the constructs pG1300 or pR1300 with C-terminal GFP or mCherry fusions to accommodate proteins of interest for transient expression assay. pR1300 was obtained by replacing GFP in pG1300 with mCherry amplified from TCV_sg2R (Zhang et al., 2017) with primers R1300-F and R1300-R (Table S3). Construct FIB-RFP was generated by inserting full-length coding sequences of *Arabidopsis* FIB2 (AT4G25630) which were obtained by RT-PCR with primers Fib2-F and Fib2-R (Table S3) into pR1300 digested with *Sal*I and *Spe*I restriction enzymes.

To generate TCV CP overexpressing transgenic lines, we constructed the binary expression vectors pCP-GFP and pSGS3-Flag with GFP and FLAG tags, respectively. Both of these are under the control of CaMV 35S promoter.

Additional details of all vectors and amplification primers are available on request.

4.3 | Y2H assay

A Gal4-based Y2H system was used to detect the interaction between various viral protein and *Arabidopsis* proteins. Approximately 100 μl of freshly prepared *Saccharomyces cerevisiae* AH109 competent cells was cotransformed with the BD and AD plasmids with the help of 5 μl of herring carrier DNA. Transformants were uniformly plated on agar-solidified double dropout (DDO) medium SD/-Leu/-Trp (SD-LW). Plates were incubated in a constant-temperature incubator at 30°C. Transformants were identified based on PCR amplification. Protein–protein interactions were detected by transferring yeast cotransformants that were grown on the DDO medium to plates containing the agar-solidified QDO medium SD/-Leu/-Trp/-His/-Ade (SD-LWHA).

4.4 | *Agrobacterium tumefaciens* infiltration and confocal microscopy

A. tumefaciens GV3101, which contained proper constructs, was infiltrated into fully expanded leaves from 3-week-old *N. benthamiana* plants at an optical density (OD_{600}) of 1.0. At 2 days post-agroinfiltration (dpa), confocal microscopy observations were carried out using an Olympus FV1000 confocal laser scanning microscope available through the Institute of Tropical Bioscience and Biotechnology, Chinese Academy of Tropical Agricultural Sciences, according to the manufacturer's protocol. The sequential mode was used when more than one fluorescence protein was expressed.

4.5 | Northern blot assay

For RNA blot analysis, total RNAs were isolated from the virus-inoculated *Arabidopsis* leaves at 5 dpi or from the upper uninoculated *Arabidopsis* leaves that were about 1 cm long at 14 dpi using TRIzol reagent (Tiangen Biotech Beijing Co., Ltd), following the manufacturer's instructions. To minimize sampling errors, we pooled leaves from six different plants (one leaf per plant) before RNA extraction. Different amounts of *Arabidopsis* total RNA were used for northern blot assay to detect vsRNAs (5 μg) and viral RNA (1 μg) according to published protocols (Wu et al., 2021; Zhang et al., 2012).

4.6 | RNA extraction, RT-qPCR, and ddPCR analysis

Total RNA was isolated using TRIzol and treated with DNase I (mona) following the manufacturer's instructions. cDNA synthesized from reverse transcription of RNA samples was used to quantify TCV accumulation levels and determine the mRNA levels of target genes. The cDNA synthesis, semiquantitative RT-PCR, and RT-qPCR assays were conducted as described previously (Wu et al., 2021; Zhang et al., 2012). The mRNA copy counts of target genes were determined using ddPCR technology with ddPCR EvaGreen Supermix (Bio-Rad Laboratories) according to the manufacturer's protocol. The ddPCR was performed in a T100 thermal cycler (Bio-Rad Laboratories) following the manufacturer's instructions. Positive droplets per microlitre sample were measured on a QX200 ddPCR droplet reader (Bio-Rad Laboratories). Based on the droplet count and according to a Poisson distribution, absolute nucleic acid copy count was calculated using QuantaSoft software (Bio-Rad Laboratories). The expression of the *AtActin1* gene was used as an internal control to normalize cDNA concentrations. Information about all the primers used is summarized in Table S5. All RT-qPCRs and ddPCRs were carried out in three independent biological replicates and triplicate for each cDNA sample.

4.7 | Protein extraction and western blot analysis

Protein was extracted from the same *N. benthamiana* leaf pool by using RIPA buffer 10 mM Tris–HCl, pH 8.0, 1 mM EDTA, 0.5 mM EGTA, 1% Triton X-100, 0.1% sodium deoxycholate, 0.1% SDS, 140 mM NaCl, 1 mM PMSF, and 1× ProBlock Gold plant protease inhibitor cocktail (the last two reagents were added immediately before use). Western blot analysis was carried out as previously

described. Anti-FLAG and anti-actin antibodies were purchased from Proteintech. Blotted membranes were washed thoroughly and visualized using ImageQuant LAS 4000mini according to the manufacturer's protocol (ECL; GE Healthcare).

4.8 | Statistical analysis

Unless otherwise stated, all experiments were performed with at least three biological replicates in all cases. Significant differences between samples in gene expression were statistically analysed with Student's tests in GraphPad Prism v. 8.0 software; values of $p < 0.05$ and $p < 0.01$ were taken as statistically significant.

ACKNOWLEDGEMENTS

We are grateful to Professor Feng Qu (Ohio State University, USA) for providing us with mutant plant lines and plasmids. We thank Dr Mengbin Ruan (Chinese Academy of Tropical Agricultural Sciences) for sharing pG1300 vector. We appreciate Professor Feng Qu (Ohio State University, USA) for critical reading of the manuscript. We thank the Public Technology Research and Sharing Center of the Institute of Tropical Bioscience and the Biotechnology Chinese Academy of Tropical Agricultural Sciences for equipment sharing and technical support. This work was supported by the Hainan Provincial Natural Science Foundation of China (321RC641, 322MS124), the National Natural Science Foundation of China (32070172 and 31570145), and the Central Public-interest Scientific Institution Basal Research Fund for the Chinese Academy of Tropical Agricultural Sciences (19CXTD-33).

DATA AVAILABILITY STATEMENT

The data that support the findings of this study and the materials used during the current study are available from the corresponding author on reasonable request.

ORCID

Xiuchun Zhang https://orcid.org/0000-0001-7720-8967

REFERENCES

Azevedo, J., Garcia, D., Pontier, D., Ohnesorge, S., Yu, A., Garcia, S. et al. (2010) Argonaute quenching and global changes in Dicer homeostasis caused by a pathogen-encoded GW repeat protein. *Genes & Development*, 24, 904–915.

Cao, M., Ye, X., Willie, K., Lin, J., Zhang, X., Redinbaugh, M.N. et al. (2010) The capsid protein of turnip crinkle virus overcomes two separate defense barriers to facilitate systemic movement of the virus in *Arabidopsis*. *Journal of Virology*, 84, 7793–7802.

Chapman, E.J., Prokhnevsky, A.I., Gopinath, K., Dolja, V.V. & Carrington, J.C. (2004) Viral RNA silencing suppressors inhibit the microRNA pathway at an intermediate step. *Genes & Development*, 18, 1179–1186.

Chen, J., Zheng, L., Shi, X., Zhang, S., Tan, X., Zhao, X. et al. (2022) The nonstructural protein NSs encoded by tomato zonate spot virus suppresses RNA silencing by interacting with NbSGS3. *Molecular Plant Pathology*, 23, 707–719.

Cheng, X. & Wang, A. (2016) The potyvirus silencing suppressor protein VPg mediates degradation of SGS3 via ubiquitination and autophagy pathways. *Journal of Virology*, 91, e01478-16.

Choi, C.W., Qu, F., Ren, T., Ye, X. & Morris, T.J. (2004) RNA silencing-suppressor function of turnip crinkle virus coat protein cannot be attributed to its interaction with the *Arabidopsis* protein TIP. *Journal of General Virology*, 85, 3415–3420.

Curtin, S.J., Watson, J.M., Smith, N.A., Eamens, A.L., Blanchard, C.L. & Waterhouse, P.M. (2008) The roles of plant dsRNA-binding proteins in RNAi-like pathways. *FEBS Letters*, 582, 2753–2760.

Dalmay, T., Hamilton, A., Rudd, S., Angell, S. & Baulcombe, D.C. (2000) An RNA-dependent RNA polymerase gene in *Arabidopsis* is required for posttranscriptional gene silencing mediated by a transgene but not by a virus. *Cell*, 101, 543–553.

Ding, S.W. (2010) RNA-based antiviral immunity. *Nature Reviews Immunology*, 10, 632–644.

Du, Z., Xiao, D., Wu, J., Jia, D., Yuan, Z., Liu, Y. et al. (2011) p2 of rice stripe virus (RSV) interacts with OsSGS3 and is a silencing suppressor. *Molecular Plant Pathology*, 12, 808–814.

Giner, A., Lakatos, L., García-Chapa, M., López-Moya, J.J. & Burgyán, J. (2010) Viral protein inhibits RISC activity by argonaute binding through conserved WG/GW motifs. *PLoS Pathogens*, 6, e1000996.

Glick, E., Zrachya, A., Levy, Y., Mett, A., Gidoni, D., Belausov, E. et al. (2008) Interaction with host SGS3 is required for suppression of RNA silencing by tomato yellow leaf curl virus V2 protein. *Proceedings of the National Academy of Sciences of the United States of America*, 105, 157–161.

Guo, H., Song, X., Xie, C., Huo, Y., Zhang, F., Chen, X. et al. (2013) Rice yellow stunt rhabdovirus protein 6 suppresses systemic RNA silencing by blocking RDR6-mediated secondary siRNA synthesis. *Molecular Plant-Microbe Interactions*, 26, 927–936.

Hiraguri, A., Itoh, R., Kondo, N., Nomura, Y., Aizawa, D., Murai, Y. et al. (2005) Specific interactions between Dicer-like proteins and HYL1/DRB-family dsRNA-binding proteins in *Arabidopsis thaliana*. *Plant Molecular Biology*, 57, 173–188.

Huang, Y.W., Hu, C.C., Tsai, C.H., Lin, N.S. & Hsu, Y.H. (2019) *Nicotiana benthamiana* Argonaute10 plays a pro-viral role in bamboo mosaic virus infection. *New Phytologist*, 224, 804–817.

Iki, T., Tschopp, M.A. & Voinnet, O. (2017) Biochemical and genetic functional dissection of the P38 viral suppressor of RNA silencing. *RNA*, 23, 639–654.

Jin, H. & Zhu, J.K. (2010) A viral suppressor protein inhibits host RNA silencing by hooking up with Argonautes. *Genes & Development*, 24, 853–856.

Jin, Y., Zhao, J.H. & Guo, H.S. (2021) Recent advances in understanding plant antiviral RNAi and viral suppressors of RNAi. *Current Opinion in Virology*, 46, 65–72.

Kumakura, N., Takeda, A., Fujioka, Y., Motose, H., Takano, R. & Watanabe, Y. (2009) SGS3 and RDR6 interact and colocalize in cytoplasmic SGS3/RDR6-bodies. *FEBS Letters*, 583, 1261–1266.

Li, F. & Wang, A. (2019) RNA-targeted antiviral immunity: more than just RNA silencing. *Trends in Microbiology*, 27, 792–805.

Li, F., Zhao, N., Li, Z., Xu, X., Wang, Y., Yang, X. et al. (2017) A calmodulin-like protein suppresses RNA silencing and promotes geminivirus infection by degrading SGS3 via the autophagy pathway in *Nicotiana benthamiana*. *PLoS Pathogens*, 13, e1006213.

Moissiard, G., Parizotto, E.A., Himber, C. & Voinnet, O. (2007) Transitivity in *Arabidopsis* can be primed, requires the redundant action of the antiviral Dicer-like 4 and Dicer-like 2, and is compromised by viral-encoded suppressor proteins. *RNA*, 13, 1268–1278.

Mourrain, P., Béclin, C., Elmayan, T., Feuerbach, F., Godon, C., Morel, J.B. et al. (2000) *Arabidopsis SGS2* and *SGS3* genes are required for posttranscriptional gene silencing and natural virus resistance. *Cell*, 101, 533–542.

Muangsan, N., Beclin, C., Vaucheret, H. & Robertson, D. (2004) Geminivirus VIGS of endogenous genes requires SGS2/SDE1 and SGS3 and defines a new branch in the genetic pathway for silencing in plants. *The Plant Journal*, 38, 1004–1014.

Okano, Y., Senshu, H., Hashimoto, M., Neriya, Y., Netsu, O., Minato, N. et al. (2014) In planta recognition of a double-stranded RNA synthesis protein complex by a potexviral RNA silencing suppressor. *The Plant Cell*, 26, 2168–2183.

Parent, J.S., Bouteiller, N., Elmayan, T. & Vaucheret, H. (2015) Respective contributions of *Arabidopsis* DCL2 and DCL4 to RNA silencing. *The Plant Journal*, 81, 223–232.

Peragine, A., Yoshikawa, M., Wu, G., Albrecht, H.L. & Poethig, R.S. (2004) SGS3 and SGS2/SDE1/RDR6 are required for juvenile development and the production of *trans*-acting siRNAs in *Arabidopsis*. *Genes & Development*, 18, 2368–2379.

Qu, F., Ren, T. & Morris, T.J. (2003) The coat protein of turnip crinkle virus suppresses posttranscriptional gene silencing at an early initiation step. *Journal of Virology*, 77, 511–522.

Qu, F., Ye, X. & Morris, T.J. (2008) Arabidopsis DRB4, AGO1, AGO7, and RDR6 participate in a DCL4-initiated antiviral RNA silencing pathway negatively regulated by DCL1. *Proceedings of the National Academy of Sciences of the United States of America*, 105, 14732–14737.

Rajamäki, M.L., Streng, J. & Valkonen, J.P. (2014) Silencing suppressor protein VPg of a potyvirus interacts with the plant silencing-related protein SGS3. *Molecular Plant-Microbe Interactions*, 27, 1199–1210.

Ruan, M.B., Guo, X., Wang, B., Yang, Y.L., Li, W.Q., Yu, X.L. et al. (2017) Genome-wide characterization and expression analysis enables identification of abiotic stress-responsive MYB transcription factors in cassava (*Manihot esculenta*). *Journal of Experimental Botany*, 68, 3657–3672.

Wang, X.B., Jovel, J., Udomporn, P., Wang, Y., Wu, Q., Li, W.X. et al. (2011) The 21-nucleotide, but not 22-nucleotide, viral secondary small interfering RNAs direct potent antiviral defense by two cooperative argonautes in *Arabidopsis thaliana*. *The Plant Cell*, 23, 1625–1638.

Weinheimer, I., Haikonen, T., Ala-Poikela, M., Moser, M., Streng, J., Rajamäki, M.-L. et al. (2016) Viral RNase3 co-localizes and interacts with the antiviral defense protein SGS3 in plant cells. *PLoS One*, 11, e0159080.

Wu, K., Wu, Y., Zhang, C., Fu, Y., Liu, Z. & Zhang, X. (2021) Simultaneous silencing of two different *Arabidopsis* genes with a novel virus-induced gene silencing vector. *Plant Methods*, 17, 6.

Yang, Z. & Li, Y. (2018) Dissection of RNAi-based antiviral immunity in plants. *Current Opinion in Virology*, 32, 88–99.

Yoshikawa, M., Peragine, A., Park, M.Y. & Poethig, R.S. (2005) A pathway for the biogenesis of trans-acting siRNAs in *Arabidopsis*. *Genes & Development*, 19, 2164–2175.

Yoshikawa, M., Iki, T., Tsutsui, Y., Miyashita, K., Poethig, R.S., Habu, Y. et al. (2013) 3′ fragment of miR173-programmed RISC-cleaved RNA is protected from degradation in a complex with RISC and SGS3. *Proceedings of the National Academy of Sciences of the United States of America*, 110, 4117–4122.

Yoshikawa, M., Han, Y.W., Fujii, H., Aizawa, S., Nishino, T. & Ishikawa, M. (2021) Cooperative recruitment of RDR6 by SGS3 and SDE5 during small interfering RNA amplification in *Arabidopsis*. *Proceedings of the National Academy of Sciences of the United States of America*, 118, e2102885118.

Zhang, X., Zhang, X., Singh, J., Li, D. & Qu, F. (2012) Temperature-dependent survival of turnip crinkle virus-infected *Arabidopsis* plants relies on an RNA silencing-based defense that requires dcl2, AGO2, and HEN1. *Journal of Virology*, 86, 6847–6854.

Zhang, X.F., Sun, R., Guo, Q., Zhang, S., Meulia, T., Halfmann, R. et al. (2017) A self-perpetuating repressive state of a viral replication protein blocks superinfection by the same virus. *PLoS Pathogens*, 13, e1006253.

Zhang, C., Chen, D., Yang, G., Yu, X. & Wu, J. (2020) Rice stripe mosaic virus-encoded P4 is a weak suppressor of viral RNA silencing and is required for disease symptom development. *Molecular Plant-Microbe Interactions*, 33, 412–422.

SUPPORTING INFORMATION

Additional supporting information can be found online in the Supporting Information section at the end of this article.

How to cite this article: Liu, L., Wang, H., Fu, Y., Tang, W., Zhao, P., Ren, Y. et al. (2023) Turnip crinkle virus-encoded suppressor of RNA silencing interacts with *Arabidopsis* SGS3 to enhance virus infection. *Molecular Plant Pathology*, 24, 154–166. Available from: https://doi.org/10.1111/mpp.13282